The effect of time delay for synchronisation suppression in neuronal networks

Matheus Hansen [a], Paulo R. Protachevicz [b], Kelly C. Iarosz [c,d], Iberê L. Caldas [b], Antonio M. Batista [e,f,*], Elbert E.N. Macau [a]

[a] *Institute of Science and Technology, Federal University of São Paulo - UNIFESP, São José dos Campos, São Paulo, SP, Brazil*
[b] *Institute of Physics, University of São Paulo, São Paulo, SP, Brazil*
[c] *Faculdade de Telêmaco Borba, FATEB, Telêmaco Borba, Paraná, Brazil*
[d] *Graduate Program in Chemical Engineering Federal Technological University of Paraná, Ponta Grossa, PR, Brazil*
[e] *Post-Graduation in Science, State University of Ponta Grossa, Ponta Grossa, PR, Brazil*
[f] *Mathematics and Statistics Department, State University of Ponta Grossa, Ponta Grossa, PR, Brazil*

ARTICLE INFO

ABSTRACT

We study the time delay in the synaptic conductance for suppression of spike synchronisation in a random network of Hodgkin–Huxley neurons coupled by means of chemical synapses. In the first part, we examine in detail how the time delay acts over the network during the synchronised and desynchronised neuronal activities. We observe a relation between the neuronal dynamics and the synaptic conductance distributions. We find parameter values in which the time delay has high effectiveness in promoting the suppression of spike synchronisation. In the second part, we analyse how the delayed neuronal networks react when pulsed inputs with different profiles (periodic, random, and mixed) are applied to the neurons. We show the main parameters responsible for inducing or not synchronous neuronal oscillations in delayed networks.

1. Introduction

The understanding of emergence, as well as the control, of neuronal synchronisation is one of the central points of contemporary neuroscience, mostly due to the fact that synchronous patterns can be related to some fundamental neuronal processes for life, such as memory [1], perception [2] and also to some brain disorders, for instance epilepsy [3]. Specifically considering the case of brain pathologies, many studies have been developed in order to find alternative methods to control synchronous neuronal activities. Protachevicz et al. [4] indicated through numerical simulations that external perturbations can not only induce peak synchronisation, but also reduce the abnormal synchronous pattern. Recently, Cota et al. [5] observed in experimental analyses with rats that non periodic electrical stimulation can be a very promising alternative for the treatment of epileptic seizures. Inspired by this scenario, this work aims to contribute to the exploration of the effects of delayed conductance on neuronal synchronisation activities. We focus on cases in which the temporal delay has a positive performance in suppressing spike synchronisation.

Different perspectives about the effect of time delay on synchronisation in complex networks have been attracting the attention of the scientific community [6]. Considering the context of neuronal communication, the time delay is an intrinsic property, being associated with axonal, dendritic, and synaptic signal propagation [7–9]. In the axons, the presence of myelination is responsible for the rapid signal transmission [10], while the demyelination causes a reduction in the conduction velocity [11]. In the chemical synapses, the time delay is between less than one millisecond and up to tens of milliseconds [12,13]. For the dendritic, the time delay is smaller than one millisecond [14].

As a model to mimic neuronal activities, we use the Hodgkin–Huxley (HH) neuron [15], which was proposed in 1952 by physiologists Alan Hodgkin and Andrew Huxley. This model was developed in a successful attempt to describe the mechanisms of action potential generation in experiments with the giant squid axon. In such a model it was reported that the generation of the action potential in the cell membrane is linked to variations in the ionic currents of potassium, sodium and a current defined by them as leak. Although various mathematical models have been proposed to reproduce the neuronal behaviour [16,17], the HH neuron is still one of the most actual approaches to neuronal dynamics, inspiring several studies in the field of neuroscience [18–20].

Our main finding in this work is to show the mechanism responsible for the emergence of spike synchronisation in networks composed of HH neurons, randomly coupled by means of chemical synapses. We explore the effects of delayed conductance on neuronal activities as an alternative method for suppressing or reducing synchronous patterns.

---

* Corresponding author at: Mathematics and Statistics Department, State University of Ponta Grossa, Ponta Grossa, PR, Brazil.
 E-mail addresses: mathehansen@gmail.com (M. Hansen), antoniomarcosbatista@gmail.com, abatista@uepg.br (A.M. Batista).

Such analyses are carried out in two different scenarios, where firstly the neuronal network has no external perturbation on the inputs, and secondly when pulse perturbations (for instance sensory stimulation) with periodic, random, and mixed profiles are considered [21]. In both cases, we discuss the conditions and parameters in which the time delay is able or not to hold low levels of spike synchronisation in neuronal networks.

The paper is organised as follows. In Section 2, we introduce the mathematical model of coupled HH neurons. In Section 3, we present the main diagnostics used in the study. In Section 4, we exhibit the suppression of synchronised activities under constant current input due to the time delay. In Section 5 shows the time delay effect under pulsed perturbed neuronal networks. Finally, we highlight the conclusions of our work in the last section.

2. Neuron model

The HH model [22] with time delay is given by

$$C\frac{dV_i}{dt} = -g_K n_i^4 (V_i - V_K) - g_{Na} m_i^3 h_i (V_i - V_{Na})$$
$$- g_1(V_i - V_1) + I_i + I_i^{syn}(t - \tau), \tag{1}$$

$$\frac{dx_i}{dt} = \alpha_{x_i}(v_i)(1 - x_i) - \beta_{x_i}(v_i)x_i, \tag{2}$$

where C is the capacitance of the cell membrane, V_i is the membrane potential for the ith HH neuron, and t is the time. The parameters g_K, g_{Na}, and g_1 correspond to the potassium, sodium, and leak maximal conductance, respectively. The variables n_i and m_i are related to the possibility of the ionic channels of potassium (K^+) and sodium (Na^+) being open (active), while h_i is associated with the possibility of the sodium channel (Na^+) being close (inactive). V_K, V_{Na}, and V_1 represent the potassium, sodium, and leak reversal potential, while I_i and I_i^{syn} correspond to the external and synaptic current density, respectively. In order to simplify the mathematical expression of opening and closing channels, we condense them as represented in Eq. (2), where x_i can be n_i, m_i, and h_i. α_{xi} and β_{xi} are different functions of v_i that depend on n_i, m_i, and h_i. In this equation, $v_i = V_i/[mV]$ represents the value of the dimensionless membrane potential. The α_{xi} and β_{xi} are experimental functions found by Hodgkin and Huxley and written as

$$\alpha_n(v_i) = \frac{0.01v_i + 0.55}{1 - \exp(-0.1v_i - 5.5)}, \tag{3}$$

$$\alpha_m(v_i) = \frac{0.1v_i + 4}{1 - \exp(-0.1v_i - 4)}, \tag{4}$$

$$\alpha_h(v_i) = 0.07 \exp\left(\frac{-v_i - 65}{20}\right), \tag{5}$$

$$\beta_n(v_i) = 0.125 \exp\left(\frac{-v_i - 65}{80}\right), \tag{6}$$

$$\beta_m(v_i) = 4 \exp\left(\frac{-v_i - 65}{18}\right), \tag{7}$$

$$\beta_h(v_i) = \frac{1}{1 + \exp(-0.1v_i - 3.5)}. \tag{8}$$

In this work, we consider that each ith HH neuron is stimulated over time by an external current density $I_i = I_i^0 + \xi(t)$, where I_i^0 is a current density with a constant amplitude and $\xi(t)$ is a pulse with amplitude Γ, which initially is equal to 0 for all times (absence of pulses), leading to $I_i = I_i^0$ (constant input). The external current density I_i is responsible for the generation of the spike dynamics. As one of our main goals is to study spike synchronisation suppression, we randomly distribute (following a uniform distribution) $I_i^0 \in [10, 14]$ μA/cm² , once in this range all HH neurons are in spike activities with inter-spike intervals (ISI) in [13, 14.6] ms [21].

The behaviour of the HH neuron is separated into two different states. The first one is the spike state which is characterised by a sudden increase in the membrane potential value. The second state is silent, in which the membrane potential exhibits a small oscillation amplitude
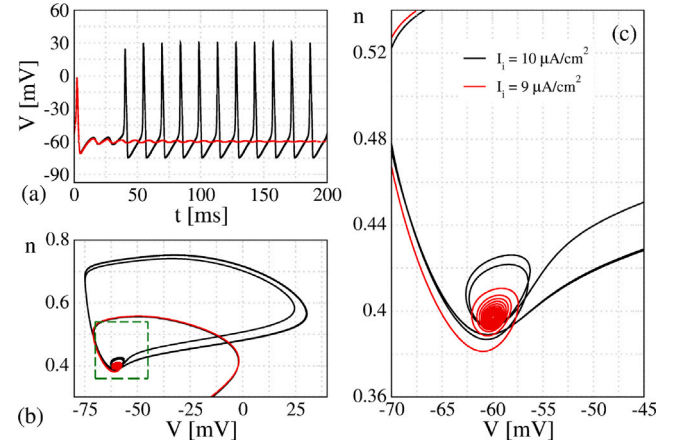

Fig. 1. (a) Representation of the spike (black line) and silent (red line) states for a single HH neuron. (b) Phase space $n \times V$ for the states displayed in panel (a). The black line indicates the limit cycle responsible for the spike dynamics and the red line is the convergence to the fixed point (silent state). (c) Magnification of the green box in the panel (b). (For interpretation of the references to colour in this figure legend, the reader is referred to the web version of this article.)

around the resting potential. These two different patterns are displayed in Fig. 1(a), where the black and red lines are the spike and silent states, respectively. The spike dynamics can be understood when the neuron solution converges to a limit cycle (LC), while the silent behaviour occurs due to convergence to a fixed point (FP). The transition from one state to another is related to a Hopf bifurcation [23,24]. Depending on the initial condition, the value of I_i can be or not enough to contribute to the bifurcation, leading the neurons from the silent to spike states. Fig. 1(b) displays the convergence to a limit cycle (black line) and a fixed point (red line) in the phase space $n \times V$. We observe that the activity of a single HH neuron i depends on the external current density I_i applied over it. Fig. 1(c) exhibits a magnification of the green box in Fig. 1(b).

We build a network composed of HH neurons coupled by means of excitatory chemical synapses. The synaptic current density received by each ith HH neuron is given by

$$I_i^{syn}(t - \tau) = (V_r^{exc} - V_i)\frac{g_{exc}}{N_i}\sum_{k=1}^{N} A_{ik} U(t - t_k - \tau) S_k(t - \tau), \tag{9}$$

where V_r^{exc} is the excitatory reversal potential, g_{exc} (mS/ cm²) is the maximal excitatory synaptic conductance, N_i is the number of excitatory connections received by the neuron i, N is the number of neurons of the neuronal network, A_{ik} is the adjacency matrix, $U(t - t_k - \tau)$ is the Heaviside function, and $S_k(t - \tau)$ is a auxiliary function which describe the temporal evolution of the synaptic conductance from the pre-synaptic neuron k to the post-synaptic neurons i. The Heaviside function is defined as

$$U(t - t_k - \tau) = \begin{cases} 1, & t > t_k + \tau, \\ 0, & t \le t_k + \tau, \end{cases} \tag{10}$$

and the $S_k(t - \tau)$ function is written as [25]

$$S_k(t - \tau) = \exp\left[-\left(\frac{t - t_k - \tau}{\tau_s}\right)\right], \tag{11}$$

where t_k represents the times in which the pre-synaptic neuron k spikes along the numerical simulation, τ is the time delay on the transmission of the synaptic conductance, and τ_s is the decay time constant on the synaptic conductance. Essentially, τ can be related to the time needed to the signal generated by the spike of the pre-synaptic neuron k to achieve the post-synaptic neuron i. Thereby, in our simulation, for $t < t_k + \tau$, we have $U \cdot S_k$ equal to 0. Fig. 2 shows the neuronal spikes for a pre-synaptic neuron k over time and their correspondent S_k generate
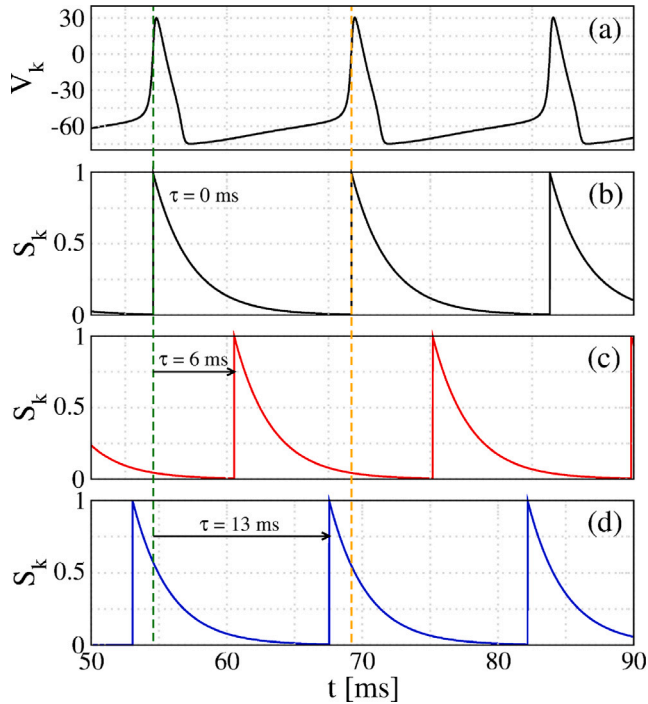
Fig. 2. Schematic representation of the synaptic conductance S_k generated by the pre-synaptic HH neuron k. In panel (a), we plot the spike dynamics for a HH neuron k. Panel (b) exhibits S_k when no time delay is considered ($\tau = 0$ ms). In panels (c) and (d), we show the effect of time delay $\tau = 6$ ms and $\tau = 13$ ms over S_k, respectively. (For interpretation of the references to colour in this figure legend, the reader is referred to the web version of this article.)

when different values of time delay are considered. In Fig. 2(a), we plot the membrane potential for neuron k. Figs. 2(b), 2(c), and 2(d) exhibit the values of S_k for $\tau = 0$ ms, $\tau = 6$ ms, and $\tau = 13$ ms, respectively. For a delay equal to zero (Fig. 2(b)), the peak of S_k matches the time in which the neuron k spikes. For delay greater than zero (Figs. 2(c) and (d)), the S_k curve is shifted to the right by the value of the time delay τ. Such effect is very significant for the system dynamics, once it indicates that the synaptic current received by the post-synaptic neuron i is not instantaneous. It is important to mention that time delays are expected for the type of connections considered in this work, given by chemical synapses. Differently from the electric synapses, in which the interactions among neurons are practically instantaneous due to the direct transfer of ions, chemical synapses depend on the release of neurotransmitters, which are associated with some delay until the post-synaptic neuron i receives the signal sent from the pre-synaptic neuron k [26].

Inspired by some works in the area that present a reasonable configuration to mimic the behaviour of a neuronal network [19,21,22,27], we build a random network composed of $N = 100$ HH neurons coupled according to Erdös–Rényi model with a probability of connection $p = 0.1$ and excluding auto-connections [28–31]. The initial conditions are randomly distributed in $V_i \in [-80, 0]$ mV and $n_i = m_i = h_i = 0$. Such a range of initial conditions is considered in order to allow the HH neurons to start their dynamics at different points from each other, i.e., conditions in which some of these neurons spike more easily than others. In our simulations, all neurons exhibit spike activities due to the chosen parameters combined with the excitatory chemical synapses, as well as with the positive external currents. The integration of the differential equations is done using the fourth-order Runge–Kutta algorithm with a fixed integration time step $\delta t = 10^{-2}$ ms [24,27,32]. A short summary of the parameters, values, ranges, and units related to the neuronal description of this work can be found along Table 1 [18,22,27].

Table 1
Description of the parameters, values, and units used in our numerical simulations.

Description	Parameter	Values
Number of neurons	N	100
Connection probability	p	0.1
Membrane capacity	C	1 µF/cm^2
Max. potassium conductance	g_K	36 mS/cm^2
Max. sodium conductance	g_{Na}	120 mS/cm^2
Max. leak conductance	g_l	0.3 mS/cm^2
Potassium reversal potential	V_K	−77 mV
Sodium reversal potential	V_{Na}	50 mV
Leak reversal potential	V_l	−54.4 mV
Exc. reversal potential	V_r^{exc}	20 mV
Exc. synaptic conductance	g_{exc}	[0,1] mS/cm^2
Const. ext. current density	I_i^0	[10,14] µA/cm^2
Period that pulse is ON	$\Delta t^{(ON)}$	[0,14] ms
Period that pulse is OFF	$\Delta t^{(OFF)}$	[0,14] ms
Adjacency matrix	A_{ik}	0 or 1
Time delay	τ	[0,14] ms
Decay time constant	τ_s	2.728 ms
Time step integration	δt	10^{-2} ms
Initial time for analyses	t_{ini}	5 s
Final time for analyses	t_{fin}	10 s

3. Diagnostics

We consider a time interval from $t_{ini} = 5$ s to $t_{fin} = 10$ s, where $t < t_{ini}$ is the transient time. In our simulation, this time interval is sufficient to perform analysis on the neuronal networks, since the system already presents stabilisation in the measurements. In order to extract an average behaviour, we compute the means over a set of 100 different numerical simulations.

3.1. Synchronisation

The diagnostic method chosen to evaluate the level of synchronicity is the mean value of the Kuramoto order parameter [33], which is calculated as

$$\langle R \rangle = \frac{1}{t_{fin} - t_{ini}} \int_{t_{ini}}^{t_{fin}} \left| \frac{1}{N} \sum_{i=1}^{N} \exp\left[j \Phi_i(t) \right] \right| dt, \tag{12}$$

where j is an imaginary number defined as $j = \sqrt{-1}$. The phase $\Phi_i(t)$ is calculated by means of

$$\Phi_i(t) = 2\pi m + 2\pi \frac{t - t_i^m}{t_i^{m+1} - t_i^m}, \tag{13}$$

where t_i^m is the time in which occurs the mth spike of the neuron i. The mean order parameter $\langle R \rangle$ is given in a range from 0 to 1, where the synchronisation is identified when $\langle R \rangle \approx 1$.

3.2. Mean synaptic current density

The synaptic current density plays an important role in the connection among the HH neurons. With this in mind, we calculate the mean synaptic current density for each time t (after a transient) as

$$\langle I^{syn}(t) \rangle = \frac{1}{N} \sum_{i=1}^{N} I_i^{syn}(t - \tau), \tag{14}$$

where $I_i^{syn}(t - \tau)$ is given by Eq. (9), while the mean value for this time interval is given by

$$\langle I^{syn} \rangle = \frac{1}{(t_{fin} - t_{ini})} \int_{t_{ini}}^{t_{fin}} \langle I^{syn}(t) \rangle dt. \tag{15}$$

3.3. Synaptic current distribution

We define a measure ζ which indicates the distribution associated with the shape of $\langle I^{syn}(t) \rangle$. The ζ measure is written as

$$\zeta = \frac{\text{mod}(H)}{\text{mean}(H)}, \tag{16}$$

where $\text{mod}(H)$ and $\text{mean}(H)$ represent, respectively, the mode and the mean value of the histogram H associated with the shape of the time series of $\langle I^{\text{syn}}(t) \rangle$. In our simulations, ζ tends to 1 if H is Gaussian-like, while ζ moves away from 1 for asymmetric and non Gaussian-like H histograms. The variation of ζ is related to the type of the synchronisation level developed by the neuronal network.

4. Time delay in unperturbed neuronal networks

For $\tau = 0$ ms and increasing the synaptic coupling g_{exc}, we observe that $\langle R \rangle$ increases, as shown in Fig. 3(a), where the neurons go from desynchronised to synchronised activities. In Figs. 3(b), 3(c), and 3(d), we plot the time series of $\langle I^{\text{syn}}(t) \rangle$ for (a) $g_{\text{exc}} = 0.01$ mS/cm^2, (b) $g_{\text{exc}} = 0.06$ mS/cm^2, and (c) $g_{\text{exc}} = 1.0$ mS/cm^2. As one can see, as greater is g_{exc}, less noisy is the shape of $\langle I^{\text{syn}}(t) \rangle$. In order to extract a characteristic of these different shapes, we compute a normalised (by the mode value) histogram H of $\langle I^{\text{syn}}(t) \rangle$ obtained during a time series of the last 5 s of the numerical simulations. Figs. 3(e), 3(f), and 3(g) display the respective histograms H associated with each $\langle I^{\text{syn}}(t) \rangle$. Comparing each one of these cases, it is possible to see that when $\langle R \rangle$ is small (Fig. 3(b)), the histogram is Gaussian-like (Fig. 3(e)). For spike synchronisation (Fig. 3(d)), the histogram has a specific shape (Fig. 3(g)), that is asymmetric and non Gaussian-like. For the intermediary case (Fig. 3(f)), for instance $\langle R \rangle = 0.49$, we see that the histogram shape changes during the transition from desynchronous to synchronous patterns. As one can see, in the synchronised activity (Fig. 3(d)), there is a higher variance on the values of the synaptic current along time, as shown in (Fig. 3(g)). On the other hand, in the desynchronised case (Fig. 3(b)), the synaptic current is maintained around a fixed value, like a Gaussian distribution (Fig. 3(e)). Through the diagnostic via ζ measure, for the cases discussed in Figs. 3(e), 3(f), and 3(g), we obtain 0.98, 0.59, and 0.03, respectively. The Gaussian-like distribution shown in Fig. 3(e) approaches 1, while another one goes away from the unit value. The complete comparison between the mean order parameter and the characterisation from the spike desynchronisation to spike synchronisation via ζ measure, when no time delay is considered, is displayed in Fig. 4(a) and 4(b) (black line). The result indicates and confirms that the mechanism involved behind the spike synchronisation, that is obtained via the increasing of g_{exc}, is linked with the alterations in the shape of $\langle I^{\text{syn}}(t) \rangle$. In addition, in Fig. 4(c), we observe that $\langle I^{\text{syn}} \rangle$ increases with g_{exc} (black line).

Now, we focus on the cases in which $\tau > 0$, denoted by the colour lines in Fig. 4. In Fig. 4(a) for $\tau \leq 1$ ms, it is possible to see a small reduction in the $\langle R \rangle$ value for larger g_{exc}. Although the time delay changes the instant that the synaptic current density arrives on the neurons, this time shift is not enough to promote relevant alteration in the collective behaviour of the HH neurons and consequently in the synchronisation. Therefore, for small time delays, the neuronal dynamics remain closer to the case without time delay. However, for $\tau \geq 2$ ms, the time shift is able to produce significant changes in the neuronal network, mainly over the mean synaptic current density, leading to a strong suppression of synchronised activities for all g_{exc} values. Fig. 4(b) shows that $\tau \geq 2$ ms increases ζ, while $\tau < 1$ ms cause only small changes. In Figs. 4(a) and 4(b), it is possible to verify that the transition between the desynchronous and synchronous states are linked once again to changes in the shape of $\langle I^{\text{syn}}(t) \rangle$, that is characterised by the ζ measure. The changes are effects of the introduction of the synaptic time delay in the neuronal connections. In Fig. 4(c), we identify a relation between the synaptic time delay and the value of $\langle I^{\text{syn}} \rangle$. As already expected, the increase of g_{exc} leads to a proportional increase of $\langle I^{\text{syn}} \rangle$, something observed (for instance) when no time delay is considered (black line). However, we also verify that when time delays are taken into account, depending on the value of τ and g_{exc}, the system can increase even more $\langle I^{\text{syn}} \rangle$ (colour lines)
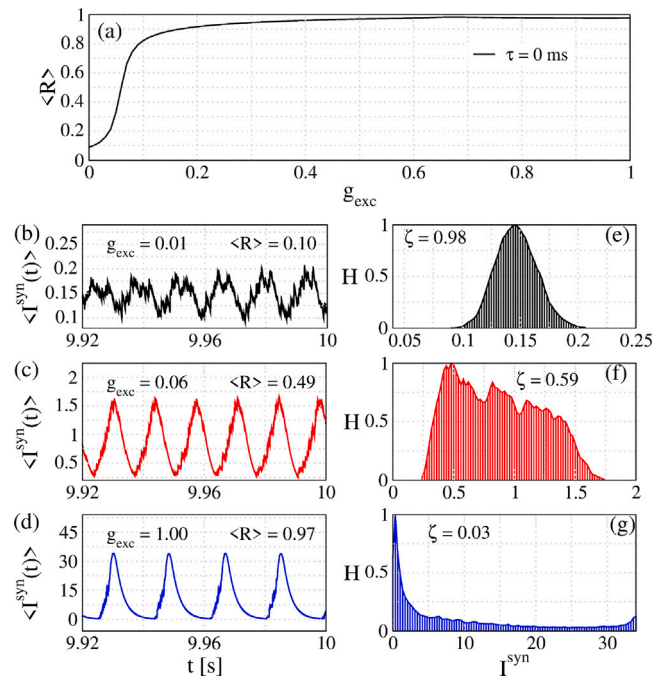

Fig. 3. (a) Mean value of the Kuramoto order parameter as a function of g_{exc}. Time series of $\langle I^{\text{syn}}(t) \rangle$ for (b) $g_{\text{exc}} = 0.01$ mS/cm^2, (c) $g_{\text{exc}} = 0.06$ mS/cm^2, and (d) $g_{\text{exc}} = 1.0$ mS/cm^2 with the respective histograms H in the panels (e), (f), and (g). We consider 100 different numerical simulations for the HH neurons and $\tau = 0$ ms.
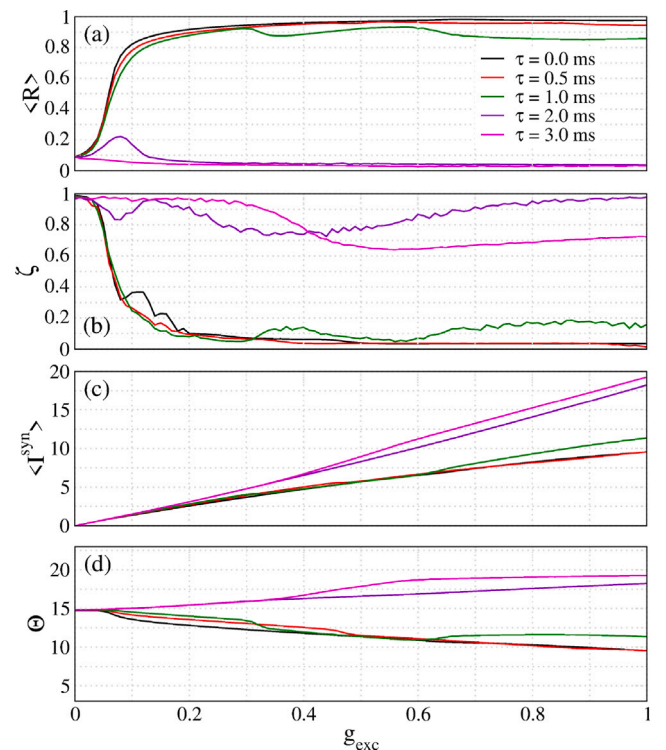

Fig. 4. Four diagnostics as a function of g_{exc} for different values of τ. (a) Mean value of the Kuramoto order parameter used in order to identify spike synchronisation of the HH neurons. (b) ζ indicates the type of the histogram obtained in the mean synaptic current $\langle I^{\text{syn}}(t) \rangle$. (c) Mean synaptic current obtained during the analyse ($\langle\langle I^{\text{syn}} \rangle\rangle$). (d) Θ represents a normalised measure defined as $\langle I^{\text{syn}} \rangle / g_{\text{exc}}$. We consider 100 different numerical simulations. (For interpretation of the references to colour in this figure legend, the reader is referred to the web version of this article.)
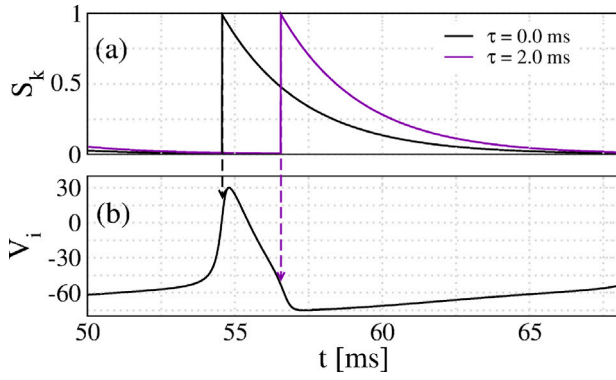
Fig. 5. Schematic representation of different times in which the synaptic conductance S_k from the pre-synaptic neuron k achieves the post-synaptic neuron i.

when compared with the case without time delay (black line). Such an increase is related to changes in the synchronisation of the HH neurons due to the introduction of the synaptic time delays. In Fig. 4(d), we present this effect through the measure Θ, which represents $\langle I^{\mathrm{syn}} \rangle$ normalised by the coupling g_{exc}. In this case, we can associate changes in the synaptic current as a consequence of the alterations promoted in the synchronisation of the neurons. As one can see, time delays which are able to desynchronise the HH neurons ($\tau \geq 2$ ms) lead to high values of Θ, which naturally will lead to the increase observed in the panel (c). A complementary explanation for such an effect also is found in Fig. 5(a), through the schematic illustration of the neuron dynamics. In this case, if for example no time delay is considered, $S_k = 1$ achieves the post-synaptic neuron i when the potential membrane is $V_i \approx 30$ mV (black dashed arrow), which makes $I_i^{\mathrm{syn}} \propto -10 \times g_{\mathrm{exc}}$ (see Eq. (9)). On the other hand, for $\tau = 2$ ms, $S_k = 1$ achieves the post-synaptic neuron i when $V_i \approx -50$ mV (violet dashed arrow), producing $I_i^{\mathrm{syn}} \propto 70 \times g_{\mathrm{exc}}$, indicating an increase of the synaptic current for the neuron i at that moment. If a similar effect occurs for more HH neurons in the network, it is reasonable to expect that, on average, $\langle I^{\mathrm{syn}} \rangle$ might have its value increased.

In Figs. 6(a), 6(b), and 6(c), we compute the parameter space $g_{\mathrm{exc}} \times \tau$, where the colour scales indicate $\langle R \rangle$, ζ, and $\langle I^{\mathrm{syn}} \rangle$, respectively. We consider $g_{\mathrm{exc}} \in [0, 1]$ mS/cm^2 and $\tau \in [0, 14]$ ms. The range of τ is chosen in order to create a link with the mean inter-spike interval (ISI) of the HH neurons in the network (about 14 ms). As can be seen in Fig. 6(a), for $0 < \tau \leq 1$ ms, the effects of the time delay are small in the synchronisation, which leads $\langle R \rangle$ to remain similar to the case in which $\tau = 0$ ms, in a way almost independently of the g_{exc}. However, for $1 < \tau \lesssim 5.5$ ms, we observe an interval of τ in which the neuronal synchronisation is suppressed for almost all g_{exc}. If $\tau > 5.5$ ms, it is also possible to verify the appearance of synchronisation. Our simulations show that there is a preferential range of the time delay in which the synchronisation can be suppressed. In Fig. 6(b), the transitions between desynchronised to synchronised spikes can be identified by means of the ζ measure, while in Fig. 6(c), it is possible to see that, depending on τ and g_{exc}, $\langle I^{\mathrm{syn}} \rangle$ can increase. For $\tau \approx 14$ ms, the parameter spaces exhibit an appearance very close to the case in which the network has no time delay. A similarity can be verified in Figs. 6(d), 6(e), and 6(f), where we compute the parameter space $g_{\mathrm{exc}} \times \tau$ in colour scale $\varepsilon^{(y)}$. The parameter $\varepsilon^{(y)}$ can be written as

$$\varepsilon^{(y)} = \frac{y(\tau) - y(0)}{\varepsilon_{\mathrm{Max}}^y}, \quad y = \langle R \rangle, \zeta, \langle I^{\mathrm{syn}} \rangle \tag{17}$$

where $y(\tau)$ represents the measure of y for $\tau > 0$, $y(0)$ is the measure of y for $\tau = 0$, and $\varepsilon_{\mathrm{Max}}^y$ corresponds to the maximum difference for this parameter with and without time delay in all considered parameter space. For instance, if we consider $y = \langle R \rangle$, $\varepsilon^{(\langle R \rangle)} \in [0, 1]$ is the difference of $\langle R \rangle$ between a network with $\tau = 0$ ms and $\tau > 0$ ms. If

$\varepsilon^{(\langle R \rangle)} \approx 0$, the network dynamics almost does not suffer changes due to the time delay. However, if $\varepsilon^{(\langle R \rangle)} \approx 1$, the opposite is observed. As indicated by Figs. 6(d), 6(e), and 6(f) for $\tau > 0$ and $\tau \leq 1$ ms, the neuronal dynamics has a high similarity with the result for τ null. For the case in which $1 < \tau < 5.5$ ms, there are relevant alterations in the neuron dynamics due to the effect of the time delay. Considering $\tau > 5.5$ ms, it is possible to observe that some parts of the parameter space exhibit similarities with the case in which no time delay is considered. Dynamically, this effect can be explained by Figs. 2(b), 2(c), and 2(d). As the time delay increases, the S_k function associated with the post-synaptic neuron i exhibits a shift in τ milliseconds. As larger is τ, further it is the S_k from the original point ($\tau = 0$ ms), indicated by the green dashed line in Fig. 2. However, for $\tau = 13$ ms, the S_k is very far from the original point (green dashed line), but it is delivered to the post-synaptic neuron i almost at the same time in which a new spike of the pre-synaptic neuron k occurs (orange dashed line). There is a kind of resonance due to the synaptic current density, indicating that even delayed, the synapse produces an equivalent effect of a neuronal network with instantaneous synaptic current density, namely a network with no time delay. Our results suggest that the values of τ, which are able to produce the suppression of synchronised activities, are in the interval $1 < \tau < 7$ ms, being more or less effective depending on g_{exc}.

In order to close this section, we provide a small and fundamental discussion about our results and the refractory period of the neuron [34]. As well known, the refractory period is a standard characteristic of the membrane neuronal evolution, and this characteristic corresponds essentially to a period in which the neuron cannot be re-excited. During the refractory period, the neuron cannot depolarise after the spike, however a neuron is still able to receive external currents, although these currents do not generate new spikes. In this work, we emphasise that the synchronisation pattern obtained for the neuronal network is not complete, so even in synchronous cases, we always have some small phase difference among the neurons, which leads them to not reach the refractory period at the same time. This point is important for our considerations, once it allows us to discuss the possibility to suppress the spike synchronisation of the HH neurons through the synaptic time delay. In order to let clear this point, in Fig. 7, we present the raster plots for the HH neurons considering different values of times delay for the neuronal network with $g_{\mathrm{exc}} = 0.5$ mS/cm^2. In the panel (a) (magnification of orange box in the panel (b)), we show a synchronised case for the neuronal network with no time delay. In such a panel, it is possible to observe that even for a $\langle R \rangle = 0.96$, the HH neurons do not spike at the same time. In the panel (c) (magnification of orange box in the panel (d)), we observe that when the time delay is short ($\tau = 1$ ms) there are just small alterations in the collective behaviour developed by the neurons ($\langle R \rangle = 0.91$). Considering $\tau = 2$ ms in the panel (e) (magnification of orange box in the panel (f)), the time delay already is able to suppress the spike synchronisation ($\langle R \rangle = 0.1$) in the neuronal network. In this situation, the time delay makes the neurons do not spike in phase synchronisation, since the input interaction does not contribute for the post-synaptic neuron firing in phase with the pre-synaptic ones, i.e, the phases of neurons are not the same and are spread in time. Finally in the panel (g) (magnification of orange box in the panel (h)), for $\tau = 14$ ms (nearly to the mean inter-spike interval (ISI)), the synchronisation returns to the neuronal network ($\langle R \rangle = 0.97$). As we observe, when time delays are associated with values around to half of the mean inter-spike interval (ISI), the synchronisation is suppressed. Once in this case the HH neurons do not spike in phase, the interactions among them do not contribute for the post-synaptic neuron fire in phase with the pre-synaptic ones.

5. Time delay effect in perturbed neuronal networks

Recently, a great interest in the effect of external perturbations in neuronal networks is getting the attention of the scientific community.
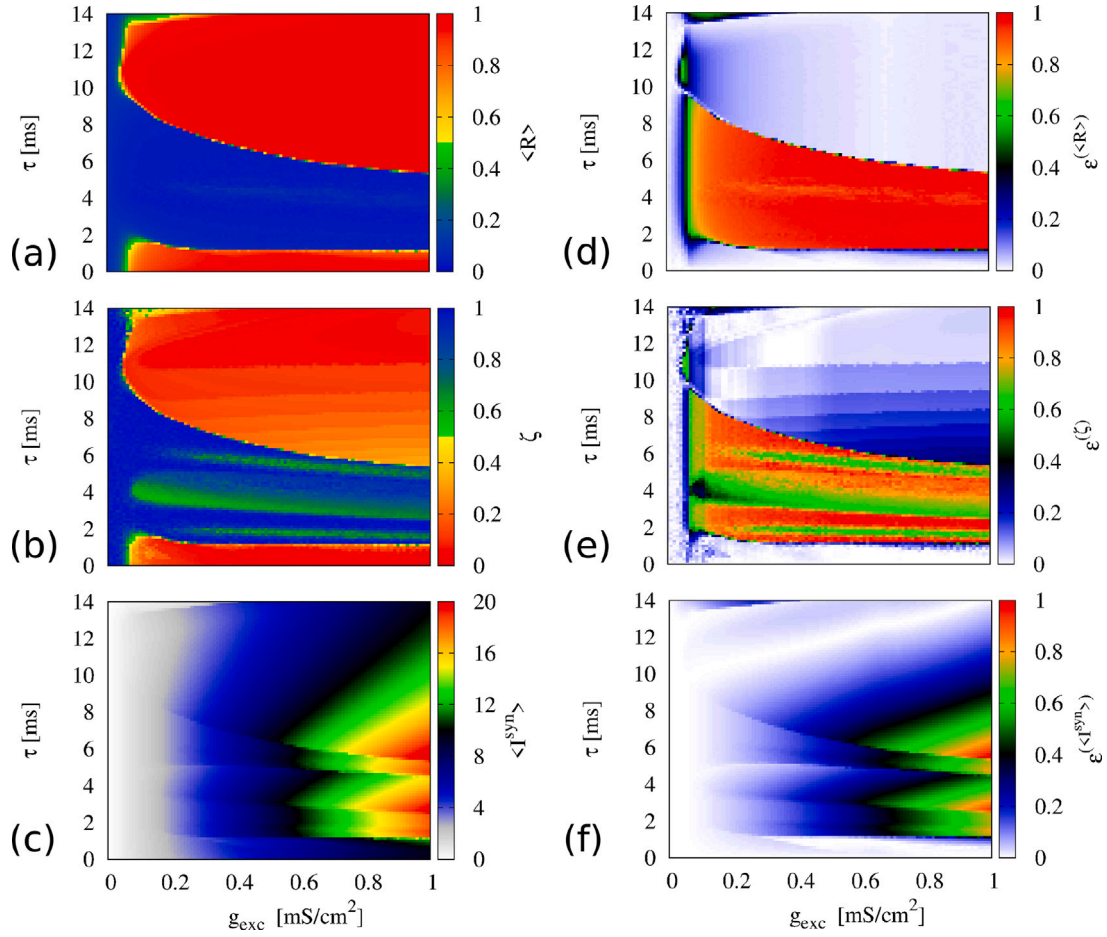
Fig. 6. Parameter space $g_{exc} \times \tau$ for (a) $\langle R \rangle$, (b) the ζ measure related to the type of the histogram H associated with $\langle I^{syn}(t) \rangle$, (c) $\langle I^{syn} \rangle$, (d) $\varepsilon^{(\langle R \rangle)}$, (e) $\varepsilon^{(\zeta)}$, and (f) $\varepsilon^{(\langle I^{syn} \rangle)}$. Depending on τ, the panels (a), (b), and (c) shows that the time delay can suppress the spike synchronisation. In the panels (d), (e), and (f), the parameter spaces indicate that there are some values of the time delay which produce similar effects than for $\tau = 0.0$ ms. (For interpretation of the references to colour in this figure legend, the reader is referred to the web version of this article.)
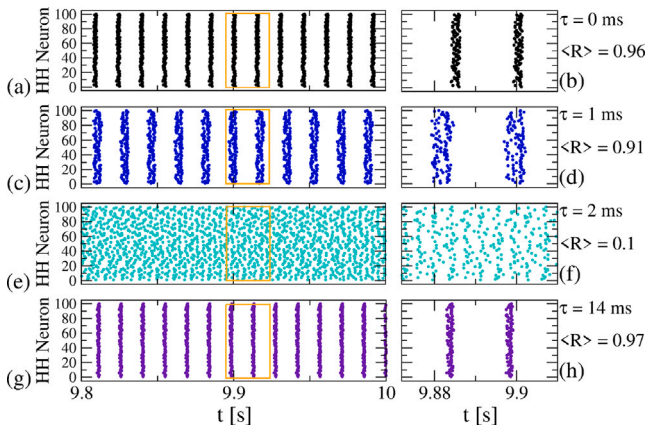
Fig. 7. Raster plots for the Hodgkin–Huxley neurons considering as time delay (a) $\tau = 0$ ms, (c) $\tau = 1$ ms, (e) $\tau = 2$ ms, and (g) $\tau = 14$ ms, with the respective magnifications of the orange box in the panels (b), (d), (f), and (h). We consider as coupled strength $g_{exc} = 0.5$ mS/cm^2 with the mean value of the Kuramoto order parameter $\langle R \rangle$ indicated in the figure for each case. (For interpretation of the references to colour in this figure legend, the reader is referred to the web version of this article.)

External perturbations can not only induce spike synchronisation, but also reduce the abnormal synchronous behaviour [4,35]. Through experimental analyses in rats, Cota et al. [5] in 2021 reported that non

periodic electrical stimulations can be a promising alternative for the treatment of epilepsy crises. Chatterjee and Robert [36] demonstrated that if some amount of noise is introduced into a stimulus, it is possible to improve the auditory perception in cochlear implants. With this in mind, we perform numerical analysis for a delayed network when three different types of pulsed perturbations (periodical, random and mixed) are introduced [21]. We study how the ranges of time delay can affect neuronal synchronous behaviour.

5.1. Periodic pulses

We begin our analysis for the case in which the pulsed perturbation is periodically applied over the neurons over time. In our simulations, we consider a perturbation $\xi(t)$ in the external current density, in order that I_i is given as

$$I_i = I_i^0 + \xi(t), \tag{18}$$

where $\xi(t)$ represents the term which assumes an amplitude equal to 0 or Γ, in an on–off configuration over time, generating a pulse profile. In the periodic pulse, the time in which the pulse is on ($\Delta t^{(ON)}$) and off ($\Delta t^{(OFF)}$) is the same. Fig. 8 displays a schematic representation of a periodic pulsed perturbation with $I_i^0 = 10$ μA/cm^2, $\Gamma = 3$ μA/cm^2 and $\Delta t^{(ON)} = \Delta t^{(OFF)} = 8$ ms.

In order to study the effect of pulsed perturbation over the neuronal network, we define two scenarios: (i) a network weakly coupled ($g_{exc} = 0.05$ mS/cm^2) and (ii) a network strongly coupled ($g_{exc} = 1.0$ mS/cm^2). An intermediary scenario ($g_{exc} = 0.5$ mS/cm^2) is also investigated,
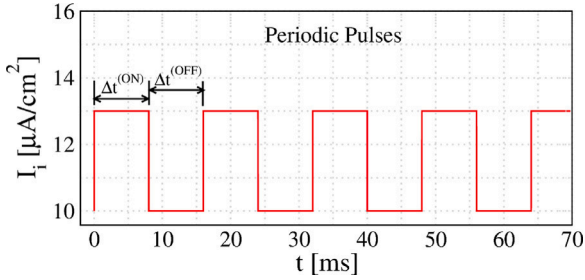
Fig. 8. Schematic representation of periodic pulses applied over $I_i^0 = 10$ μA/cm^2, considering a pulse amplitude $\Gamma = 3$ μA/cm^2 and $\Delta t^{(ON)} = \Delta t^{(OFF)} = 8$ ms.

however, the numerical results found can be, without loss of generality, approached to the case (ii). In both scenarios, we apply the pulsed perturbation with a Γ amplitude, where the associated time interval assumes $\Delta t^{(ON)} = \Delta t^{(OFF)} = \Delta t \in [0, 14]$ ms. The pulses assume the on–off configurations in scales around the mean inter-spike interval (ISI) of the HH neurons in the network.

Figs. 9(a), 9(b), and 9(c) display $\langle R \rangle$ in the parameter space $\Delta t \times \tau$ for a weakly coupled, where we consider $\Gamma = 1$ μA/cm^2, $\Gamma = 3$ μA/cm^2, and $\Gamma = 10$ μA/cm^2, respectively. If Δt is approximately lower than 2 ms, the periodic pulses are not able to alter the dynamic of the network, independently of the Γ value. However, when $\Delta t > 2$ ms, it is possible to observe spike synchronisation due to the pulsed perturbations. Increasing the pulse amplitude, the range around $\Delta t \sim 7$ ms begins to be more relevant to induce spike synchronisation. In this case, the interval of each cycle (on-off) of the pulse perturbation, approximately, coincides with the mean inter-spike interval (ISI), i.e., $2\Delta t$ (14 ms)=$\Delta t^{(ON)}$ (7 ms) + $\Delta t^{(OFF)}$ (7 ms) $\approx$ ISI (14 ms). This fact is clear in Fig. 9(a), where small amplitudes of pulsed perturbation are sufficient to induce synchronisation for $\Delta t \sim 7$ ms. In Fig. 9(c), where $\Gamma = 10$ μA/cm^2, we find ranges approximately in $5 < \Delta t < 8$ ms in which the pulse is able to induce all the HH neurons in spike synchronisation, for all τ considered in this study.

Figs. 9(d), 9(e), and 9(f) display $\langle R \rangle$ in $\Delta t \times \tau$ for strong coupling and the same Γ amplitudes considered in the weak coupling. In Figs. 9(d), we observe that $\Gamma = 1$ μA/cm^2 induces only small regions of the spike synchronisation in the parameter space for Δt around 7 ms. Therefore, under strong coupling, the neuronal network exhibits a greater resistance or a lesser influence of small external perturbations. On the other hand, as the amplitude Γ increases, the perturbation starts to be more capable to induce spike synchronisation, as shown in Figs. 9(e) and 9(f). As can be seen in Fig. 9(f) for $\Gamma = 10$ μA/cm^2, there is a large continuous range of $6 < \Delta t < 10$ ms which reduces the capacity to observe desynchronised spikes for some delays.

The periodic pulses can reduce the range of the time delay which are able to suppress spike synchronisation in weakly and strongly coupled neurons. However, such reduction depends on the time intervals in which the pulses are applied. Our results suggest that for the appropriate time intervals $\Delta t^{(ON)}$ and $\Delta t^{(OFF)}$, the transition from desynchronised activities to synchronised ones can be done by pulses with high or low amplitude, indicating that these parameters of the pulse have a crucial role in the alterations of the collective neuronal behaviour.

5.2. Random pulses

We consider a pulsed perturbation according to a random protocol for the choice of the time in which the pulses are on–off. We define that $\Delta t^{(ON)}$ and $\Delta t^{(OFF)}$ are randomly chosen (following a uniform distribution) in $[0, 14]$ ms. Fig. 10 exhibits a schematic representation of the random pulses over time for $I_i^0 = 10$ μA/cm^2 and $\Gamma = 3$ μA/cm^2, where $\Delta t^{(ON)}$ and $\Delta t^{(OFF)}$ assume random values.

In order to study the effects of random pulses in the neuronal dynamics, we compute the parameter space. Fig. 11(a), 11(b), and 11(c) display $\langle R \rangle$ in the parameter space $g_{exc} \times \tau$ for $\Gamma = 1$ μA/cm^2, $\Gamma = 3$ μA/cm^2, and $\Gamma = 10$ μA/cm^2, respectively. For $\Gamma = 1$ μA/cm^2, the neuronal network has no significant alterations, independently of g_{exc} or τ used in this work. If the pulse amplitude is increased to $\Gamma = 3$ μA/cm^2, the network begins to exhibit some changes, however, only for small values of g_{exc}. In this case, the random pulses can improve the level of spike synchronisation in the delayed neuronal network approximately for $\tau < 2$ ms and $\tau > 10$ ms. On the other hand, as g_{exc} increases, the synchronisation does not show any remarkable changes, indicating a difference between the periodic and random pulses. For the periodic case and appropriate time intervals (Figs. 9(a), 9(b), 9(d), and 9(e)), the pulses with $\Gamma = 1$ μA/cm^2 and $\Gamma = 3$ μA/cm^2 are enough to promote alterations in the networks with weak and strong couplings. In Fig. 11(c), if $\Gamma = 10$ μA/cm^2, there are more synchronised ranges in the parameter space, including in strong couplings, which is not verified for random pulses with small amplitudes (Figs. 11(a) and 11(b)).

In Fig. 12, we show the behaviour associated with the spike synchronisation and the amplitude Γ of the pulses through the parameter space $g_{exc} \times \Gamma$ for $\tau = 7$ ms. Small pulse amplitudes ($\Gamma < 1$ μA/cm^2) are not capable of promoting remarkable changes in the Hodgkin–Huxley neurons and consequently in the collective behaviour developed by them, a fact also previously displayed by Fig. 11(a). However, if the amplitude is increased, the pulses become significant and induce neuronal synchronisation, as can be observed for $\Gamma > 1$ μA/cm^2. When $\Gamma \approx 10$ μA/cm^2 and for almost all parameters, low level of synchronisation (approximately $g_{exc} < 0.35$ mS/cm^2) is replaced by at least a partial synchronisation, while the synchronised regions (approximately $g_{exc} > 0.35$ mS/cm^2) are maintained by the random pulses. In our simulations, we consider different time delays τ, and our results corroborate with our initial statement about the emergence of spike synchronisation in delayed networks when random pulses with high amplitudes are considered.

As suggested along this section, the random pulses can also reduce ranges of τ associated with desynchronised activities in the parameter space. However, such reduction is related to the amplitude values of the pulses. For the random pulses, Γ needs to assume large values in order to induce synchronised regions along the parameter space. For the periodic pulses, even small amplitudes of Γ, if applied in appropriate time intervals, are enough to change the neuronal dynamics.

5.3. Mixed pulses

We consider that the mixed perturbation is composed of sequential time windows λ_P and λ_R, where the pulses are assumed as periodic and random, respectively. In our numerical simulations, we define the relation about the sizes of these time windows as

$$\lambda_P = \lambda_P^0 - \lambda_R, \tag{19}$$

where λ_P^0 and λ_R are the sizes of the time window for the periodic and random pulses, respectively. For $\lambda_R = 0$ ms, the pulse is formed only by sequences of windows $\lambda_P = \lambda_P^0$, configuring a complete periodic pulse. On the other hand, if we consider $\lambda_R > 0$ ms, the perturbation is composed of alternating sequence windows, λ_P and λ_R, where the pulses assume the periodical and random profiles, respectively. Consequently, if $\lambda_R = \lambda_P^0$, only random pulses are observed, once there are no time windows λ_P in the signal. In Fig. 13, we show a sketch of these mixed pulses for $I_i^0 = 10$ μA/cm^2, $\Gamma = 3$ μA/cm^2, $\Delta t^{(ON)} = \Delta t^{(OFF)} = 8$ ms (for the periodic part of the pulse), $\lambda_P = 20$ ms, and $\lambda_R = 10$ ms.

In order to analyse the transition from a complete periodic pulse to a random one, we consider $\Delta t^{(ON)} = \Delta t^{(OFF)} = 8$ ms, $\Gamma = 10$ μA/cm^2, and $\lambda_P^0 = 200$ ms. In Fig. 14, we calculate the parameter space $\lambda_R \times \tau$ with $\langle R \rangle$ in colour scale. When the network is perturbed only by periodic pulses ($\lambda_R = 0$ ms), the region of desynchronised spike activity is reduced. For complete random pulses ($\lambda_R = 200$ ms), there are more
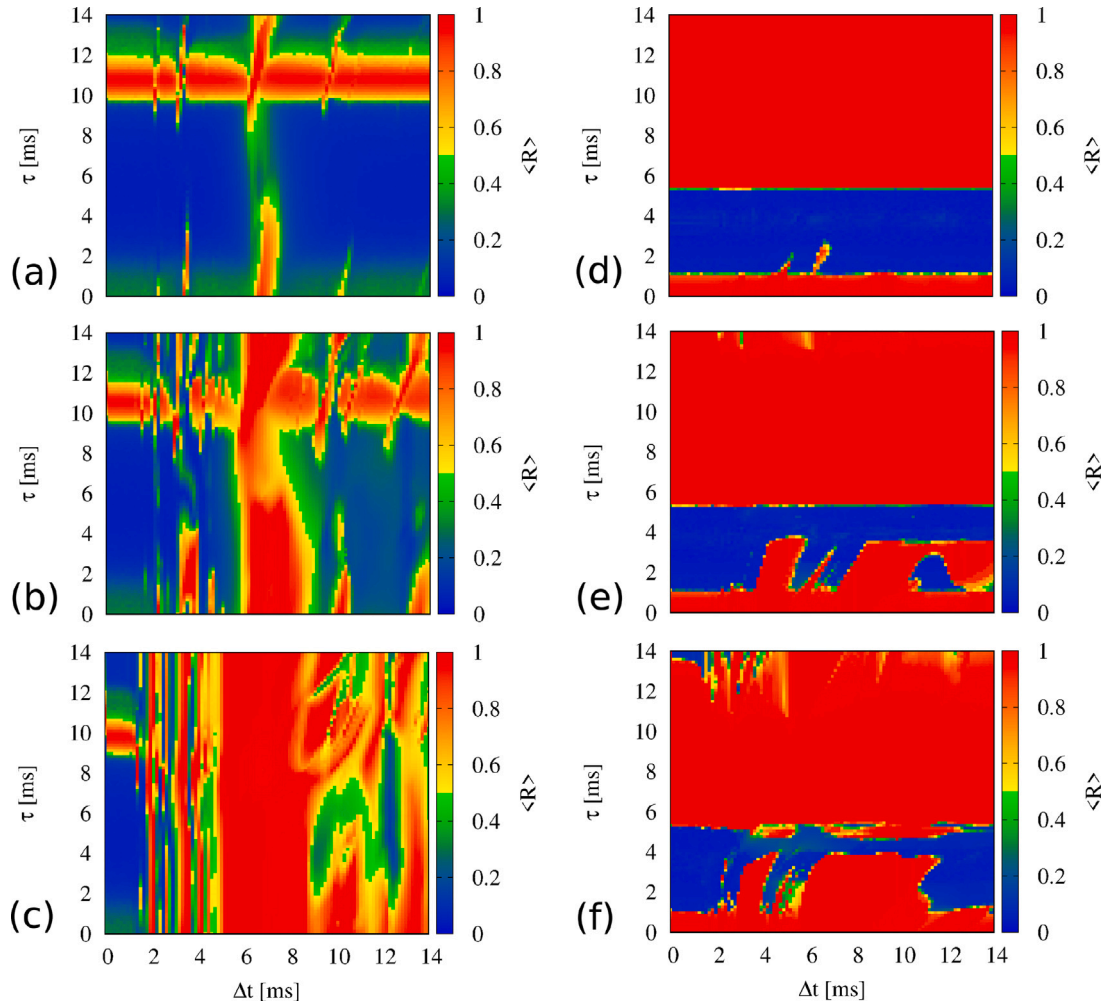
Fig. 9. Parameter space $\Delta t \times \tau$ with the mean value of the Kuramoto order parameter $\langle R \rangle$ in colour scale. In the panels (a), (b), and (c), we show an analyse for a scenario of weak coupling ($g_{exc} = 0.05$ mS/cm^2) in which the HH neurons are perturbed by periodic pulses with amplitude $\Gamma = 1$ μA/cm^2, $\Gamma = 3$ μA/cm^2, and $\Gamma = 10$ μA/cm^2, respectively. In the panels (d), (e), and (f), we consider the same pulse amplitudes, respectively, however, considering a scenario of strong coupling ($g_{exc} = 1.0$ mS/cm^2). Depending on Δt, we observe that the periodic perturbation is able to reduce the ranges in which τ has high effectiveness on the suppression of synchronised activities, even when a small amplitude of the pulse is considered. For $\Delta t \sim 7$ ms, the interval of each cycle (on-off) of the pulse perturbation, approximately, coincides with the mean inter-spike interval (ISI), i.e., $2\Delta t$ (14 ms)=$\Delta t^{(ON)}$ (7 ms) + $\Delta t^{(OFF)}$ (7 ms) $\approx$ ISI (14 ms), creating a kind of resonance that might be inducing spike synchronisation. (For interpretation of the references to colour in this figure legend, the reader is referred to the web version of this article.)
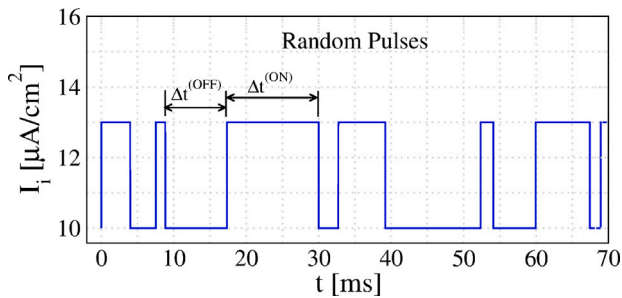
Fig. 10. Schematic representation of the random pulse dynamics applied over $I_i^0 = 10$ μA/cm^2, considering $\Gamma = 3$ μA/cm^2 with $\Delta t^{(ON)}$ and $\Delta t^{(OFF)}$ randomly chosen (following a uniform distribution) in [0; 14] ms.
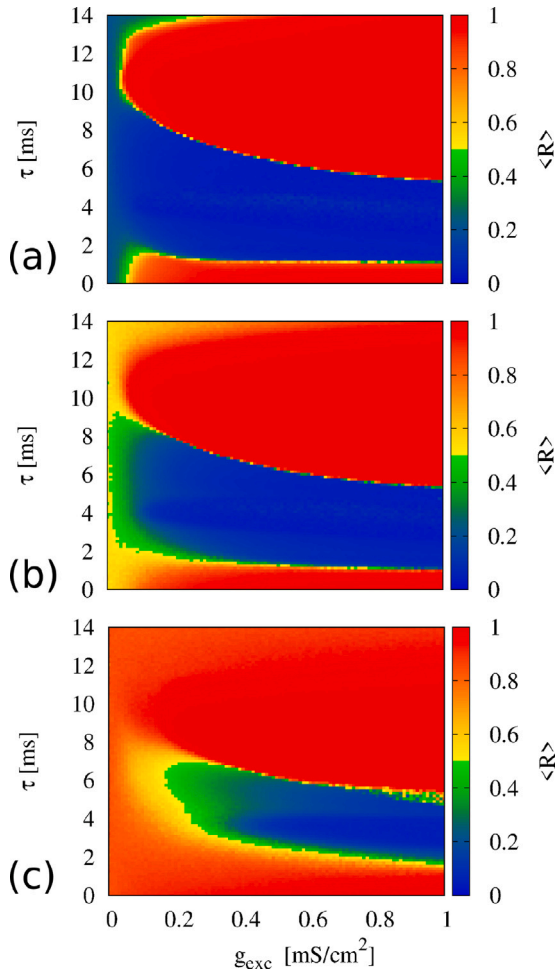
values of τ that are able to suppress spike synchronisation. We find that $\lambda_R \approx 5$ ms is enough to change the parameter space in order to increase the interval of τ in which occurs suppression of spike synchronisation. Increasing λ_R, the range of τ becomes larger. Moreover, as indicated by our numerical simulation for this case, the transition between a complete periodic pulse to a random one is given in a smooth way.

Our results indicate that small windows of random pulses embedded in a sequence of periodic ones can be enough to influence the neuronal dynamics more like a random perturbation than a periodic one. The neurons behave more similarly to the case in which the network is under random perturbations. This analyse is interesting and complements a recent observation which indicates that the same effects appear in a scenario of weak coupling [21].

6. Conclusions

In this work, we study the effects of time delays in the synaptic conductance as a way to suppress spike synchronisation developed in coupled Hodgkin–Huxley neurons. The time delays in the synaptic conductance are related to no instantaneous transmission of the synaptic currents between the neurons. Depending on the time delay and coupling strength values, changes in the synaptic current can induce or not spike synchronisation. Our results show that there is an important range of time delays ($\tau > 1$ until $\tau \approx 5.5$ ms) in which the synchronised activities are suppressed, independently of the coupling strength value.
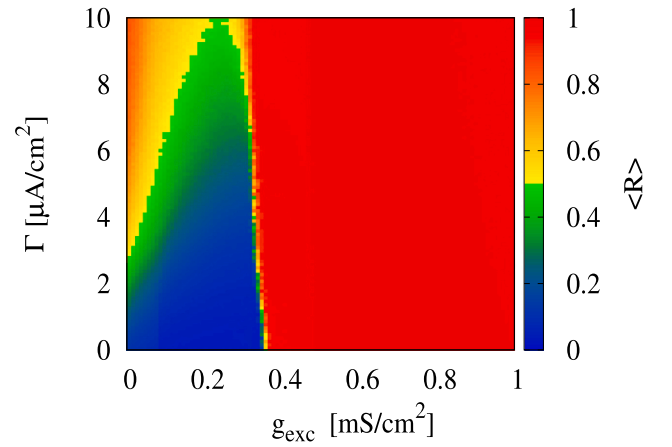
We analyse how a delayed neuronal network behaves when pulsed perturbations are applied to the neurons. Our results indicate that both periodic and random pulses can reduce the intervals of the time

Fig. 12. $\langle R \rangle$ (colour scale) in the parameter space $g_{exc} \times \Gamma$ for $\tau = 7$ ms. Increasing Γ, the random pulses become more significant and determinant in the induction of neuronal synchronisation in the delayed network. For $\Gamma \approx 10$ μA/cm^2, almost all parameters in which low level of synchronisation is found (approximately $g_{exc} < 0.35$ mS/cm^2) are replaced by at least a partial synchronisation, while the synchronised regions (approximately $g_{exc} > 0.35$ mS/cm^2) are maintained by the random pulses. (For interpretation of the references to colour in this figure legend, the reader is referred to the web version of this article.)
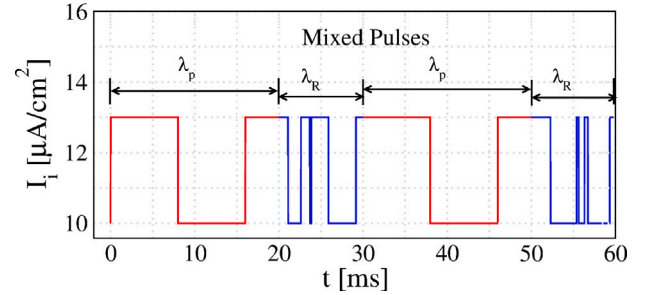
Fig. 13. Schematic representation of the mixed pulse for $I_i^0 = 10$ μA/cm^2, taken into account a pulse amplitude $\Gamma = 3$ μA/cm^2. We consider a $\lambda_P = 20$ ms with $\Delta t^{(ON)} = \Delta t^{(OFF)} = 8$ ms for the periodic part of the pulse. In the random part, we consider $\lambda_R = 10$ ms with $\Delta t^{(ON)}$ and $\Delta t^{(OFF)}$ randomly chosen in $[0, 14]$ ms.

Fig. 11. Parameter space $g_{exc} \times \tau$ with the mean value of the Kuramoto order parameter $\langle R \rangle$ in colour scale. In the panels (a), (b), and (c), we plot an analyse for the parameter space when random pulses with amplitude $\Gamma = 1$ μA/cm^2, $\Gamma = 3$ μA/cm^2, and $\Gamma = 10$ μA/cm^2 are applied over the HH neurons, respectively. We see that the random perturbation is able to reduce the ranges in which τ has high effectiveness on the suppression of synchronised activities. However, differently of the periodic case, the random pulses need to assume Γ with larger amplitudes in order to promote changes in the delayed network. (For interpretation of the references to colour in this figure legend, the reader is referred to the web version of this article.)

Fig. 14. Parameter space $\lambda_R \times \tau$ with the mean value of the Kuramoto order parameter $\langle R \rangle$ in colour scale. We see the transition from a complete periodic pulsed perturbation ($\lambda_R = 0$ ms) to a fully random pulsed perturbation ($\lambda_R = 200$ ms). For $\lambda_R \approx 5$ ms, the mixed pulse begins to induce effects characteristic of random pulses. (For interpretation of the references to colour in this figure legend, the reader is referred to the web version of this article.)

delay values in which the spike synchronisation is suppressed. For appropriate time intervals, the periodic pulses are able to generate synchronisation in the presence of time delays associated with desynchronised activities, even for pulses with small amplitudes. In this case, we find a type of resonance related to the intervals of pulsed cycles close to the mean inter-spike interval (ISI) of the HH neurons. For the random case, alterations in the synchronisation can be only observed for larger amplitudes of the pulses. Our simulations demonstrate that if small windows of random pulses are embedded in a sequence of periodic pulses, the mixed perturbations can exhibit similar characteristics to the random pulses.
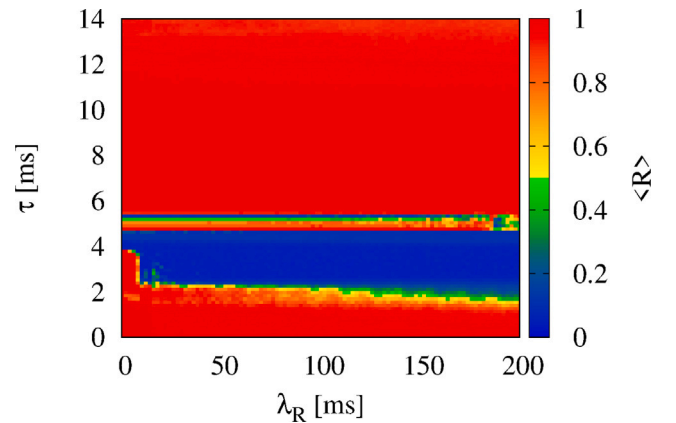
Considering that spike synchronisation can be associated with some brain pathologies, such as epilepsy, then the search for alternative methods that aim to avoid synchronous patterns are needed. As suggested by our findings in this work, the time delay can be an approach to reduce or even avoid spike synchronisation in generic Hodgkin–Huxley neuronal networks, especially if the time delay is from $\tau > 1$ ms to $\tau \approx 5.5$ ms. Besides, such results also complement the current literature involving neuronal delayed networks, once our results are in agreement with previously observed effects in networks composed of Rulkov neurons [37]. In addition, such an interval is also capable of

holding desynchronised spikes even for some perturbation conditions applied over the HH neurons, which is an important result due to

the fact that perturbations can be associated for instance with some sensory stimulus. In such a scenario, the delay might be part of the important steps toward to finding a useful and applicable method to control synchronised activities, mostly considering that time delay is a common effect in chemical synapses. In this way, interventions that can change the time of neuronal transmission could bring new possibilities for synchronisation control.

CRediT authorship contribution statement

Matheus Hansen: Discussed the results, Contributed to the final version of the manuscript. **Paulo R. Protachevicz:** Discussed the results, Contributed to the final version of the manuscript. **Kelly C. Iarosz:** Discussed the results, Contributed to the final version of the manuscript. **Iberê L. Caldas:** Discussed the results, Contributed to the final version of the manuscript. **Antonio M. Batista:** Discussed the results, Contributed to the final version of the manuscript. **Elbert E.N. Macau:** Discussed the results, Contributed to the final version of the manuscript.

Declaration of competing interest

The authors declare that they have no known competing financial interests or personal relationships that could have appeared to influence the work reported in this paper.

Data availability

Data will be made available on request.

Acknowledgements

References

[1] Gruber MJ, Hsieh L-T, Staresina BP, Elger CE, Fell J, Axmacher N, et al. Theta phase synchronization between the human hippocampus and prefrontal cortex increases during encoding of unexpected information: A case study. J Cogn Neurosci 2018;30:1646–56.

[2] Jamal W, Das S, Maharatna K, Pan I, Kuyucua D. Brain connectivity analysis from EEG signals using stable phase-synchronized states during face perception tasks. Physica A 2015;434:273–95.

[3] Traub RD, Wong RKS. Cellular mechanisms of neuronal synchronization in epilepsy. Science 1982;216:745–7.

[4] Protachevicz PR, Borges FS, Lameu EL, Ji P, Iarosz KC, Kihara AH, et al. Bistable firing pattern in a neural network model. Front Comput Neurosci 2019;13:1–19.

[5] Cota VR, de Oliveira JC, Damázio LCM, Moraes MFD. Nonperiodic stimulation for the treatment of refractory epilepsy: Applications, mechanisms, and novel insights. Epilepsy Behav 2021;121:106609.

[6] Boccaletti S, Pisarchik AN, del Genio CI, Amann A. Synchronization: from coupled systems to complex networks. Cambridge University Press; 2018.

[7] Asl MM, Valizadeh A, Tass PA. Dendritic and axonal propagation delays determine emergent structures of neuronal networks with plastic synapses. Sci Rep 2017;7:39682.

[8] Asl MM, Valizadeh A, Tass PA. Dendritic and axonal propagation delays may shape neuronal networks with plastic synapses. Front Physiol 2018;9:1–8.

[9] Protachevicz PR, Borges FS, Iarosz KC, Baptista MS, Lameu EL, Hansen M, et al. Influence of delayed conductance on neuronal synchronization. Front Physiol 2020;11:1053.

[10] Seidl AH. Regulation of conduction time along axons. Neurosci 2014;274:126–34.

[11] Waxman SG. Conduction in myelinated, unmyelinated, and demyelinated fibers. Arch Neurol 1977;34:585–9.

[12] Purves D, Augustine GJ, Fitzpatrick D, Hall WC, LaMantia A-S, Mooney RD, et al. Neuroscience. 6th Ed.. New York: Sinauer Associates; 2018.

[13] Stoelzel CR, Bereshpolova Y, Alonso J-M, Swadlow HA. Axonal conduction delays, brain state, and corticogeniculate communication. J Neurosci 2017;37:6342–58.

[14] Spencer MJ, Grayden DB, Bruce IC, Meffin H, Burkitt AN. An investigation of dendritic delay in octopus cells of mammalian cochlear nucleus. Front Comp Neurosci 2012;6:1–19.

[15] Hodgkin AL, Huxley AF. A quantitative description of membrane current and its application to conduction and excitation in nerve. J Physiol 1952;117:500–44.

[16] Rulkov NF. Modeling of spiking–bursting neural behavior using two-dimensional map. Phys Rev E 2002;65:041922.

[17] Protachevicz PR, Hansen M, Iarosz KC, Caldas IL, Batista AM, Kurths J. Emergence of neuronal synchronisation in coupled areas. Front Comput Neurosci 2021;15:663408.

[18] Popovych OV, Tass PA. Control of abnormal synchronization in neurological disorders. Front Neurol 2014;5:268.

[19] Borges FS, Protachevicz PR, Lameu EL, Bonetti RC, Iarosz KC, Caldas IL, et al. Synchronised firing patterns in a random network of adaptive exponential integrate-and-fire neuron model. Neural Netw 2017;90:1–7.

[20] Pisarchik AN, Hramov AE. Multistability in physical and living system. Springer Cham; 2022, Edition number 1.

[21] Hansen M, Protachevicz PR, Iarosz KC, Caldas IL, Batista AM, E.E.N. Macau EEN. Dynamics of uncoupled and coupled neurons under an external pulsed current. Chaos Solitons Fractals 2022;155:111734.

[22] Lameu EL, Borges FS, Iarosz KC, Protachevicz PR, Antonopoulos CG, Macau EEN, et al. Short-term and spike-timing-dependent plasticity facilitate the formation of modular neural networks. Commun Nonlinear Sci Numer Simul 2021;96:105689.

[23] Keener J, Sneyd J. Mathematical physiology. New York: Springer; 1998.

[24] Andreev AV, Frolov NS, Pisarchik AN, Hramov AE. Chimera state in complex networks of bistable Hodgkin–Huxley neurons. Phys Rev E 2019;100:022224.

[25] Lameu EL, Macau EEN, Borges FS, Iarosz KC, Caldas IL, Borges RR, et al. Alterations in brain connectivity due to plasticity and synaptic delay. Eur Phys J Spec Top 2018;227:673–82.

[26] Northrop RB. Introduction to dynamic modeling of neuro-sensory systems. In: Biomedical engineering series, CRC Press; 2001.

[27] Borges RR, Borges FS, Lameu EL, Batista AM, Iarosz KC, Caldas IL, et al. Effects of the spike timing-dependent plasticity on the synchronisation in a random Hodgkin–Huxley neuronal network. Commun Nonlinear Sci Numer Simul 2016;34:12–22.

[28] Bollobás B. Random graphs. 2nd ed.. Cambridge University Press; 2001.

[29] Frieze A, Karonski M, Michal. Introduction to random graphs. Cambridge University Press; 2015.

[30] Borges FS, Protachevicz PR, Pena RFO, Lameu EL, Higa GSV, Kihara AH, et al. Self-sustained activity of low firing rate in balanced networks. Physica A 2020;537:122671.

[31] Protachevicz PR, Iarosz KC, Caldas IL, Antonopoulos CG, Batista AM, Kurths J. Influence of autapses on synchronization in neuronal networks with chemical synapses. Front Syst Neurosci 2020;14:604563.

[32] Butcher JC. A history of Runge–Kutta methods. Appl Numer Math 1996;20:247–60.

[33] Acebrón JA, Bonilla LL, Vicente CJP, Ritort F, Spigler R. The kuramoto model: A simple paradigm for synchronization phenomena. Rev Modern Phys 2005;77:137–85.

[34] Arbib MA. The handbook of brain theory and neural networks. 2nd ed.. Cambridge, Massachusetts, London, England: The MIT Press; 2002.

[35] Jesus SD, Okun MS, Foote KD, Martinez-Ramirez D, Roper JA, Hass RJ, et al. Square biphasic pulse deep brain stimulation for Parkinson's disease: The BiP-PD study. Front Hum Neurosci 2019;13:368.

[36] Chatterjee M, Robert ME. Noise enhances modulation sensitivity in cochlear implant listeners: Stochastic resonance in a prosthetic sensory system? J Assoc Res Otolaryngol 2001;02:159–71.

[37] Sausedo-Solorio JM, Pisarchik AN. Synchronization in network motifs of delay-coupled map-based neurons. Eur Phys J Special Topics 2017;226:1911–20.